Science

MAAS

Supplementary Materials for

Multilegged matter transport: A framework for locomotion on noisy landscapes

Baxi Chong *et al*.

Corresponding author: Daniel I. Goldman, daniel.goldman@physics.gatech.edu

The PDF file includes:

Materials and Methods
Supplementary Text
Figs. S1 to S6
References

Other Supplementary Material for this manuscript includes the following:

Movie S1

1 Materials and Methods

1.1 Terrain construction

To systematically emulate rugose terrains, we used stepfields in accordance with NIST standards for assessing search-and-rescue robot capabilities *(32)*. Each block is a 10 by 10 cm square with a height between 0 and 12 cm in 1 and 2.5 cm increments for the terrains with rugosity $R_g = 0.17$ and $R_g = 0.32$, respectively. The number of blocks associated with each height was determined from a normal distribution generated in MATLAB. We obtain two terrains with a mean and standard deviation of 6.0 and 2.0 cm for the $R_g = 0.17$ terrain and 6.25 and 4 cm for the $R_g = 0.32$ terrain. We truncate these distributions between 0 and 12 cm using MATLAB's truncate() command such that we avoided negative heights in our model and extreme heights when physically constructing these terrains. We formed these blocks out of foam (FOAMULAR Insulating Sheathing (IS) XPS Insulation) and laid them spatially across a 2D grid of size W, H where $(W, H) = (80, 160)$ cm for the $R_g = 0.17$ terrain and (50, 300) cm for the $R_g = 0.32$ terrain.

We placed the blocks such that we would avoid extreme height differences (≥ 8 cm) as that would require active lifting across the body and would thus classify these terrains as a different form of terradynamic interaction than that we wish to test. The procedure we followed is detailed below.

We denote the starting height distribution of blocks as H_0, the total number of blocks as N, and the distribution after some number M of blocks have been placed as H_M. We begin the act of populating the grid by placing a block of 0 height at location $(1, 1)$. That forms our base case that allows us to implement the more general process of determining arbitrary block height after M blocks have been placed. To determine what height the $M +$ 1 block should be at a location (x, y), we look to each neighboring block of that position

according to a Manhattan distance metric. These block heights are denoted as h_1, h_2, h_3, and h_4. Note that along the edges of the grid when $x, y = 0$ or W, H respectively, there will be less neighbors according to how many edges this (x, y) location touches and we denote the total number of neighbors as n. We then generate n distributions of height differences by subtracting these neighboring block heights from the remaining height distribution and denote these new distributions as Δ_i where $\Delta_i = H_M - h_i = \delta_1, \delta_2, ..., \delta_M$. From these sets, we discard all $|\delta_i| \geq \delta_{lim}$ where δ_{lim} is our chosen height difference limit of 8 cm. These new sets are denoted as $\Delta_{i,s}$. We then add the corresponding neighboring block height to each of these sets $(H_{i,s} = \Delta_{i,s} + h_i)$ and generate a final set of heights $H_{M,f}$ made up of blocks that appear within each $H_{i,s}$ ($H_{M,f} = H_{1,s}$ & $H_{2,s}$ & $H_{3,s}$ & $H_{4,s}$). From $H_{M,f}$, we randomly choose a height according to a uniform distribution and place that at location (x, y). We repeat this process until the grid is populated, iterating along x until W is met after which y is incremented by 1 and x is reset to 0.

1.2   Robophysical experiments

Modular design   We built a robotic system composed of repeating units *(16)* such that we can vary the spatial redundancy to robophysically test our theoretical predictions for multi-legged locomotion. Each part of the robot was 3D-printed on a Taz Workhorse using PolyLite Polylactic Acid (PLA) as the printing material. We used Dynamixel 2XL430-W250 and AX-12A motors to control body undulation and limb retraction/protraction, respectively. An example of a body module is shown in Fig. S1.A and it consists of 4 active degrees of freedom (DoF).The leg up/down motor (AX12A) controls the contact states of contralateral limbs and the leg swing motor (AX12A) controls the fore/aft positions (θ) of those same limbs. Each leg is hinged to the hip connector using a rigid DoF revolute joint whose rotation axis is parallel to the fore/aft direction. The legs can lift up to $60°$
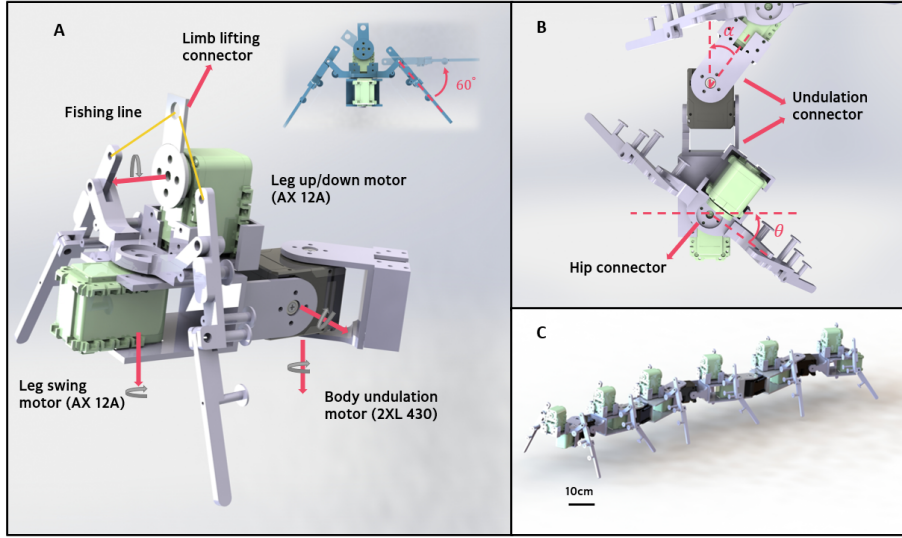
Figure S1: **Robophysical model**. (A) CAD of one module of the robot. The legs are out-of-phase and their up/down and fore/aft positions are controlled by two AX 12A motors. The body motor (2XL 430) controls the lateral undulation and vertical waves of the body. (B) Body angle and legs are coupled to each other with hip and undulation connectors. Inset shows the max lifting angle (60°) of the leg. (C) Overall sketch of a 12-legged robot.

from their neutral position which corresponds to a maximum lift of about 7cm above the ground (see the inset of the Fig. S1.A). The 2XL430-W250 motor controls the lateral (α, the yaw joint) and vertical (the pitch joint) body movements and connects to the leg motors via an undulation connector (Fig. S1.B). The final design of a module (length = 15 cm) with three servos is given in Fig. S1. This modular design allows us to readily change the number of the modules (and legs) of the robot. We perform experimental verification of our prediction model by changing modules of the robophysical model (3 to 8 modules corresponding to 6 to 16-legged robotics system).

Compliant leg features Inspired by centipede observations and past robophysical studies, we leverage elastic restoring forces using rubber bands (Alliance Rubber 26324 Advantage Rubber Bands Size 32) to incorporate two types of leg compliance on the

robot that mitigate the effects of parallel force disturbances. The first design is an inward leg compliance demonstrated in Fig. S2.A. We connect the leg up/down motor to each contralateral limb pair using fishing line (RIKIMARU Braided Fishing Line Abrasion Resistant Superline Zero Stretch, yellow lines in Fig. S1.A), thus coupling the legs such that as one is raised, the other lowers to the ground. During operation, this servo tensions the cord to vertically raise the desired limb while slackening the cord on the other side. This results in the contralateral leg lowering to the ground, aided by the rubber bands mounted at the hip connector. This "stepping leg" lowers until the opposing ground force is equal to the elastic force, thereby allowing the robot height to be non-uniform across the body in the presence of obstacles.

The second design is the longitudinal leg compliance demonstrated in Fig. S2.B. It consists of a rotational pivot and rubber band that connect the upper and lower parts of the leg, effectively forming a "knee" at each limb. This design enables the legs to passively bend and drag across encountered obstacles, thus mitigating substantial parallel force disruptions. Once past the obstructions, the rubber band restores the leg to its neutral straight position such that locomotion can continue as normal.

Robophysical experiment procedure We use the Dynamixel SDK library in MAT-LAB to program and control our robophysical model. During experiments, we keep the robot tethered on two cords. One supplies the recommended servo voltage of 11.1 V from a DC HY3050E power supply while the other connects to the PC via Robotis U2D2 (Fig. S3). We place retroreflective markers on each leg up/down motor of the robot and track their motion during trials using 4 OptiTrack Prime 13w mounted on tripods at each corner of the testing arena (Fig. S4). Afterwards, we use the Motive software to process the data and export the results to MATLAB for further analysis.
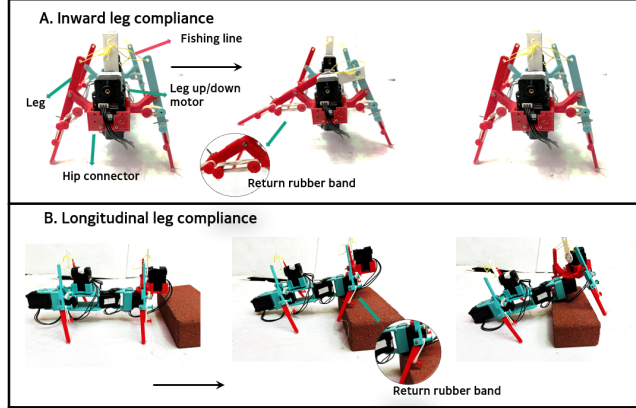
Figure S2: **Compliant leg features**.(A) Working principle of inward compliance. Return rubber bands connect legs and the hip connector. Drag forces from rubber bands support the weight of each module of the robot. Rubber bands also recover the lifted leg to its neutral position when the leg up/down motor stops lifting. (B) Working principle of the directional flexible (bends from head to tail) leg with a return rubber band. The leg approaches the obstacle, pivots around the tip, and bends. After it passes the obstacle, the rubber band returns the leg to its neutral position. Black arrow indicates the moving direction of the robot.

We measured the average velocity by recording the net displacement (of the head module) over T periods. Similarly, we measured the transport duration by recording the time required for robot (head module) to move some distance D.

1.3   Contact planning

We use a binary variable c to represent the contact state of a leg, where $c = 1$ represents the stance phase and $c = 0$ represents the swing phase. Following *(30)*, the contact pattern of robophysical model with N pairs of legs can be written as

$$
\begin{aligned}
c_l(\tau_c, 1) &= \begin{cases} 1, & \text{if } \mathrm{mod}(\tau_c, 2\pi) < 2\pi D \\ 0, & \text{otherwise} \end{cases} \\
c_l(\tau_c, i) &= c_l(\tau_c - 2\pi \frac{\xi}{N}(i-1), 1) \\
c_r(\tau_c, i) &= c_l(\tau_c + \pi, i),
\end{aligned} \tag{S.1}
$$
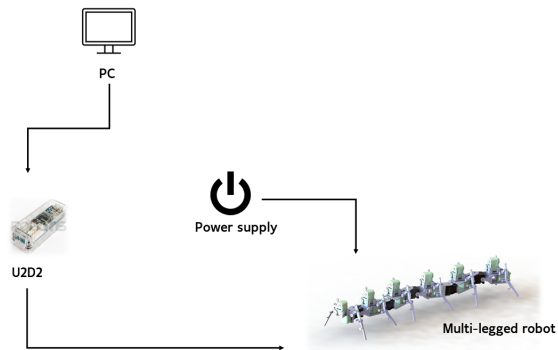
Figure S3: **Robot connection**. The PC input control signals to the robot via a Robotis U2D2 USB communication converter. A DC power supply HY3050E provides power for the motors.
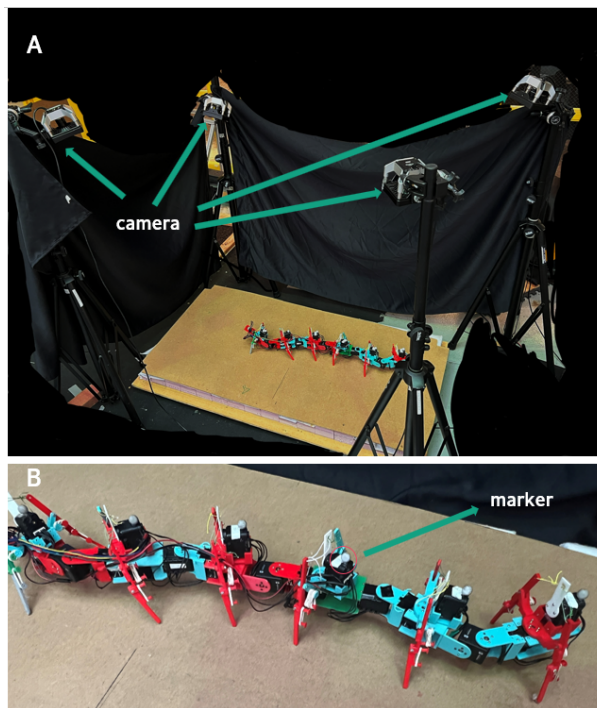
Figure S4: **Tracking system setup**. (A) Four 4 OptiTrack Prime 13w cameras are fixed on tripods and placed at each corner of the testing arena for tracking. (B) A 12-legged robot mounted with markers.
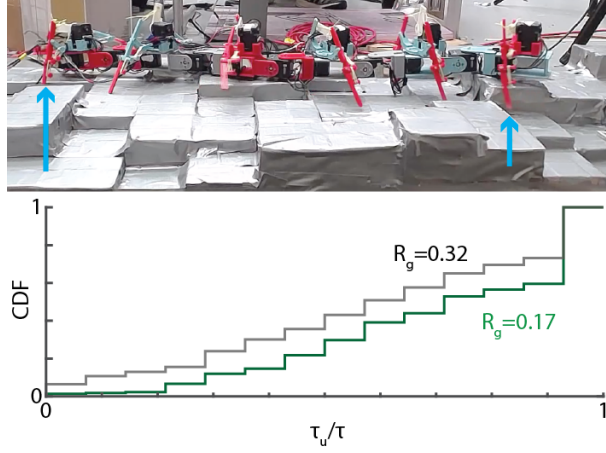
Figure S5: **Contact error**. (*Top*) Side view of robot on rugose terrain. Missing steps are identified in blue arrows. (*Bottom*) Cumulative distribution functions of empirically measured contact duration for (green) lower rugose terrain with $R_g = 0.17$ and (black) higher rugose terrain with $R_g = 0.32$

where ξ denotes the number of spatial waves on the legs, D is the duty factor, and $c_l(\tau_c, i)$ (and $c_r(\tau_c, i)$) denotes the contact state of the i-th leg on the left (and the right) at gait phase τ_c, $i \in \{1, ...N\}$ for $2n$-legged systems (See Fig. S1).

Legs generate self-propulsion by protracting during the stance phase, and retracting during the swing phase. That is, the leg moves from the anterior to the posterior end during the stance phase and moves from the posterior to anterior end during the swing phase. With this in mind, we use a piece-wise sinusoidal function to prescribe the anterior/posterior angles (θ) for a given contact phase (τ_c) defined earlier,

$$\theta_l(\tau_c, 1) = \begin{cases} \Theta_{leg} \cos\left(\frac{\tau_c}{2D}\right), & \text{if } \mathrm{mod}(\tau_c, 2\pi) < 2\pi D \\ -\Theta_{leg} \cos\left(\frac{\tau_c - 2\pi D}{2(1-D)}\right), & \text{otherwise,} \end{cases}$$

$$\theta_l(\tau_c, i) = \theta_l(\tau_c - 2\pi\frac{\xi}{N}(i-1), 1)$$

$$\theta_r(\tau_c, i) = \theta_l(\tau_c + \pi, i) \tag{S.2}$$

where Θ_{leg} is the shoulder angle amplitude, and $\theta_l(\tau_c, i)$ and $\theta_r(\tau_c, i)$ denote the leg shoulder angle of i-th left and right leg at contact phase τ_c, respectively. Note that the shoulder

8

angle is maximum ($\theta = \Theta_{leg}$) at the transition from swing to stance phase, and is minimum ($\theta = -\Theta_{leg}$) at the transition from stance to swing phase. Note that we chose $D = 0.5$ unless otherwise mentioned.

We then introduce lateral body undulation by propagating a wave along the backbone from head to tail, The body undulation wave is

$$\alpha(\tau_b, i) = \Theta_{body}\cos(\tau_b - 2\pi\frac{\xi^b}{N}(i-1)), \tag{S.3}$$

where $\alpha(\tau_b, i)$ is the angle of the i-th body joint at phase τ_b and ξ^b denotes the number of spatial waves on the body. For simplicity, we assume that the spatial frequency of the body undulation wave and the contact pattern wave are the same, i.e. $\xi^b = \xi$.

In this way, gaits of multi-legged locomotors can be characterized by the superposition of a body wave and a leg wave. As discussed in *(30)*, the optimal body-leg coordination (optimal phasing of body undulation to assist leg retraction) is $\phi_c = \tau_b - (\xi/N + 1/2)\pi$. In this paper, we took $\Theta_{leg} = \pi/6$, $\Theta_{body} = \pi/6$, $\xi = N/6$ for all experiments.

1.4 Gait design and bac kinematics

For our analysis, we consider myriapod gaits that follow the prescriptions detailed above. The instantaneous thrust is given by *(27)*:

$$f(t) = \sin\left(\tan^{-1}\frac{v_y(t)}{v_x(t)}\right) \text{ if } t \in (0, \tau)$$

where

(A) Side view

t=0

t=T/2

t=T

(B) Top view

t=0

t=T/2

t=T
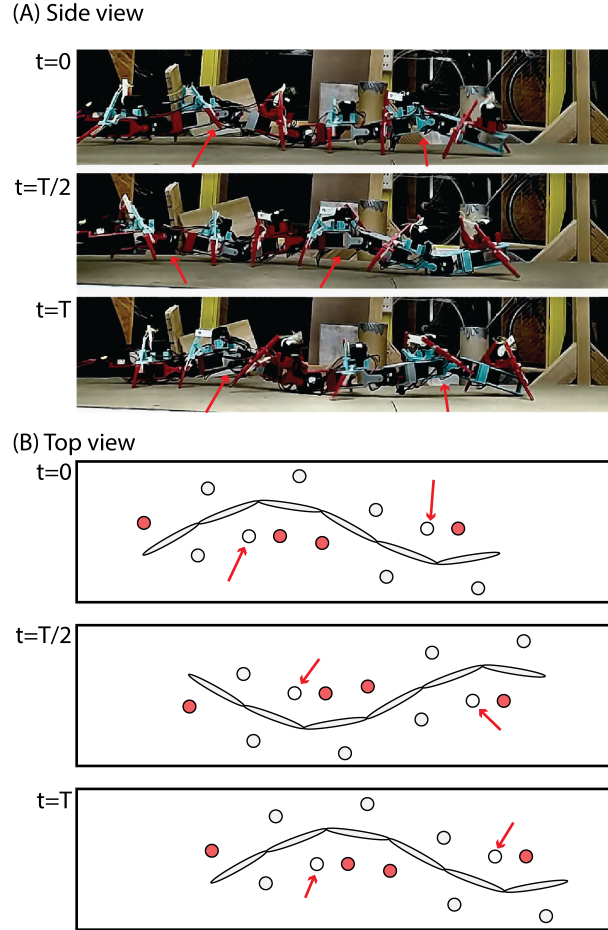
Figure S6: **Contact modulation**. Snapshots of (A) side view and (B) top view of contact modulated gaits. Note that for modules in the concave part of the vertical wave (labelled in red arrow), both legs are not in contact with the substrate because of contact modulation. We also label the modules in the concave part of the vertical wave in the top view.

$$v_x(t) = x_m \cos(2\pi \frac{t}{2\tau}) - l\gamma_m \sin(2\pi \frac{t}{2\tau}) \sin(\gamma_m \cos(2\pi \frac{t}{2\tau}))$$

$$v_y(t) = l\gamma_m \sin(2\pi \frac{t}{2\tau}) \cos(\gamma_m \cos(2\pi \frac{t}{2\tau}))$$

$$\gamma_m = \tan^{-1}(2\pi \xi x_m) + \Theta_{leg}$$

$$x_m = N\Theta_{body}/(4\pi^2 \xi^2)$$

Note that l is the ratio between leg length and body length. For modules with fixed leg length, we have $l = \frac{l_{leg}}{Nl_{body}}$, where l_{leg} is the leg length and l_{body} is the module length.

In our framework, we consider the case where $t > \tau$ (e.g., $\tau_u + c_1 > \tau$). In those cases, we define the actual bac to have two segments: $[0, \ c_1 + \tau_u - \tau] \cup [c_1, \ \tau_u]$. In this way, we define $f(t)$ to be periodic: $f(t) = f(t + k\tau), \ k \in \mathbb{Z}$.

Proposition 1. $f(t)$ *is independent of the number of leg pairs* N.

Proof. By re-arranging the terms in the definition of x_m we find that

$$\gamma_m = \tan^{-1}(3\Theta_{body}/\pi) + \Theta_{leg},$$

which is independent of N.

Additionally we can rewrite v_x as:

$$
\begin{aligned}
v_x(t) &= x_m \cos(2\pi \frac{t}{2\tau}) - l\gamma_m \sin(2\pi \frac{t}{2\tau}) \sin(\gamma_m \cos(2\pi \frac{t}{2\tau})) \\
&= \frac{9\Theta_{body}}{\pi^2 N} \cos(\frac{\pi t}{\tau}) - \frac{\gamma_m l_{leg}}{Nl_{body}} \sin(\frac{\pi t}{\tau}) \sin(\gamma_m \cos(\frac{\pi t}{\tau})) \\
&= \frac{1}{N} g_x(t),
\end{aligned}
$$

where $g_x(t)$ is a function that does not depend on N.

Similarly, we have:

$$
\begin{aligned}
v_y(t) &= l\gamma_m \sin(2\pi \frac{t}{2\tau}) \cos(\gamma_m \cos(2\pi \frac{t}{2\tau})) \\
&= \frac{l_{leg}}{Nl_{body}} \gamma_m \sin(2\pi \frac{t}{2\tau}) \cos(\gamma_m \cos(2\pi \frac{t}{2\tau})) \\
&= \frac{1}{N} g_y(t),
\end{aligned}
$$

where $g_y(t)$ is a function that does not depend on N.

In all, we find that $\frac{v_y(t)}{v_x(t)}$ is independent of N, which implies that $f(t)$ is independent of N.

$\square$

The nominal velocity, v_{open} has the following property (27):

$$\int_0^\tau \sin\left(\tan^{-1}\frac{v_y(t) - v_{open}}{v_x(t)}\right)dt = 0.$$

Proposition 2. *The absolute velocity is independent of the number of leg pairs N.*

Proof. Note that v_{open} has units of body lengths per cycle. The body length is given by Nl_{body}. Therefore, the absolute velocity is given by $v_{abs} = v_{open} \times Nl_{body}$.

In this way, we have:

$$\int_0^\tau \sin\left(\tan^{-1}\frac{v_y(t) - v_{open}}{v_x(t)}\right)dt$$
$$= \int_0^\tau \sin\left(\frac{\frac{1}{N}g_y(t) - \frac{1}{N}\frac{v_{abs}}{l_{body}}}{\frac{1}{N}g_x(t)}\right)dt$$
$$= \int_0^\tau \sin\left(\frac{g_y(t) - \frac{v_{abs}}{l_{body}}}{g_x(t)}\right)dt = 0.$$

since both $g_x(t)$ and $g_y(t)$ are independent of N, we know that v_{abs} is also independent to N.

$\square$

The thrust-velocity relationship is given by:

$$\hat{f} - f_n = \frac{1}{\tau}\int_0^\tau \sin\left(\tan^{-1}\frac{v_y(t) - v}{v_x(t)}\right)dt,$$

where $f_n = \frac{1}{\tau}\int_0^\tau \sin\left(\tan^{-1}\frac{v_y(t)}{v_x(t)}\right)dt$ is the nominal thrust.

12

1.5 Contact modulation

We modulate the contact duration by imposing a vertical body wave. This wave is implemented by the vertical joints $\alpha_v(i)$. The vertical wave and lateral wave are coupled in the following way:

$$\alpha_v(\tau_b, i) = \Theta_v \cos(2\tau_b - 4\pi \frac{\xi^b}{N}(i-1)). \tag{S.4}$$

Observe that the vertical wave has a spatial frequency twice that of the lateral wave. The modules in the concave part of the vertical wave are lifted off the ground (Fig. S6) so that both legs are not in contact with the substrate. This contact modulation scheme follows similar coordination patterns as the sinus lifting as discovered in snakes *(46)*. Snapshots of contact modulation are illustrated in Fig. S6.

2 Supplementary Text

In this paper, we only need to consider the sign function $\text{sign}(x)$ for $x \geq 0$. It is defined as follows:

$$\text{sign}(x) = \begin{cases} 1, & \text{if } x > 0 \\ 0, & \text{if } x = 0 \end{cases}$$

Proposition 3. *$\hat{f} = \text{sign}(\tau_u)\tau_u^{-1}f_u$, as defined in Eq. 1, is sampled from a probability density function. Then*

$$\hat{f}_T^{[1]} = \frac{1}{T}\sum_{i=1}^{T}\hat{f}$$

converges in probability to a constant random variable $\langle \hat{f} \rangle$. This is equivalent to saying that $\hat{f}_T^{[1]}$ tends, as T approaches infinity, to a Dirac delta function supported at $\langle \hat{f} \rangle$. Similarly, $\hat{v} = \gamma^{-1}\hat{f}$ also tends to a Dirac delta function as T tends to infinity.

Proof. The convergence in probability follows directly from the Law of Large Numbers. Observe that $\hat{f}_T^{[1]}$ is the average of T independent identically distributed random variables, X, each having finite variance independent of T. Suppose that $\mathrm{Var}(X) = \sigma^2$, and let X^T denote the random variable given by $(X+...+X)/T$ (T summands). Then $\hat{f}_T^{[1]}$ has variance given by $\mathrm{Var}(X^T) = \sigma^2/T$. This variance converges to 0 as T approaches infinity, which implies that $X^\infty = \lim_{T\to\infty} X^T$ is a constant random variable with probability 1.

Let $\langle \hat{f} \rangle$ denote the mean of $\hat{f}$. Then the mean of X^T will be $T\langle \hat{f} \rangle/T = \langle \hat{f} \rangle$, independent of T. Hence X^∞ will also have mean $\langle \hat{f} \rangle$. $\square$

Proposition 4. *Consider $\hat{v}_T^{[N]}$, as defined in Eq. 2. Define $\hat{v}^{[N]} = \hat{v}_1^{[N]}$. As N tends to infinity, $\hat{v}^{[N]}$ tends to a Dirac delta function. Further, $\langle \hat{v}^{[N]} \rangle$ can be approximated by $(1 - b^N)C_s$ when N is large, where C_s is a constant determined by $f(t)$, γ and b.*

Proof. Recall that $p(\tau_u \leq 0)$ is given by $G(0) = b$, and the definition of G precedes Eq. 1 in the text. We consider the complete missing step ($\sum_{j=1}^{N} \tau_u^j = 0$) in Eq. 2. The probability of complete missing step is then b^N, and in this case we define $\hat{v}^{[N]} = 0$. Thus, $\langle \hat{v}^{[N]} \rangle$ can be expressed by:

$$\langle \hat{v}^{[N]} \rangle = b^N \times 0 + \frac{1 - b^N}{\gamma} \left\langle \frac{\sum_{j=1}^{N} f_u^j}{\sum_{j=1}^{N} \tau_u^j} \right\rangle \tag{S.5}$$

We must analyze the quotient of random variables in this expression.

Let us define two new random variables

$$P_N = \frac{1}{N} \sum_{j=1}^{N} f_u^j$$

$$Q_N = \frac{1}{N} \sum_{j=1}^{N} \tau_u^j.$$

14

Note that both P_n and Q_n represent the sample mean of the random variables f_u and τ_u, respectively.

Each of the τ_u are identical independently distributed random variables having finite mean $\langle \tau_u \rangle = \frac{1-b}{2}\tau$. Hence we apply the (weak) law of large numbers to conclude that as $N \to \infty$ the sample mean Q_N converges in mean to a constant random variable $Q = \frac{1-b}{2}\tau$.

In a similar way, we ovserve that the f_u are identical independently distributed random variables having finite mean $\langle f_u \rangle$. So by the (weak) law of large numbers, we conclude that the sample mean P_N converges in probability to the constant random variable $P = \langle f_u \rangle$.

Finally, by the Cramér's rule (see theorem 11.4 in *(47)*), the random variable P_N/Q_N converges in distribution to the constant random variable $P/Q = \langle f_u \rangle / ((1-b)\tau/2) = \frac{2\langle f_u \rangle}{\tau(1-b)}$. Define a constant

$$C_s = \frac{2\langle f_u \rangle}{\gamma \tau (1-b)}.$$

Now, by equation (S.5), we have proved that

$$\langle \hat{v}^{[N]} \rangle = \frac{1-b^N}{\gamma} \left\langle \frac{\sum_{j=1}^{N} f_u^j}{\sum_{j=1}^{N} \tau_u^j} \right\rangle \to (1-0) \cdot C_s \tag{S.6}$$

as $N \to \infty$.

The statement that P_N/Q_N converges in distribution to a constant random variable is equivalent to the statement that the random variable $\hat{v}^{[N]}$ tends, as $N \to \infty$, to a Dirac delta function supported at C_s.

$\square$

Proposition 5. *Consider a matter transportation task to deliver a payload over distance D at the scheduled time of arrival $T = kD$, where k^{-1} is the nominal speed. Define the matter transportation task to be successful if the actual displacement $\hat{D}$ (evaluated at T) satisfies $|D - \hat{D}| < \epsilon$. Consider the case of exact delivery where $\epsilon = 0$. To guarantee*

successful matter transportation with probability p_0, "the minimal spatial redundancy" is bounded by:

$$N_{p_0} \leq \frac{\log(1 - p_0^{1/(kD)})}{\log(b)}$$

Proof. Recall that the distribution of terrain-disturbed velocity is defined as:

$$\hat{v} = \gamma^{-1} \operatorname{sign}(\tau_u)\tau_u^{-1} f_u$$

where the distribution of τ_u is illustrated in Fig. 3.A.2 right panel; $f_u^i = \int_{c_1}^{c_1 + \tau_u} f(t)dt$. Clearly, the distribution of $\hat{v}$ is dependent on the thrust generation function $f(t)$. We consider a simple choice of $f(t)$ which allows us to derive a bound for N_{ϵ, p_0}. Specifically, we consider the case where $f(t)$ is constant over time. We then have:

$$p(\hat{v} = k^{-1}) = 1 - b$$

$$p(\hat{v} = 0) = b \tag{S.7}$$

where k^{-1} is the nominal velocity, and $b > 0$ is the probability of a complete bac loss. Now we consider the terrain-disturbed velocity with spatial redundancy N:

$$\hat{v}^{[N]} = \frac{1}{\gamma} \operatorname{sign}\left(\sum_{i=1}^{N} \tau_u^i\right) \frac{\sum_{i=1}^{N} f_u^i}{\sum_{i=1}^{N} \tau_u^i},$$

Following the assumption that $f(t)$ is constant over time, we know that $\hat{v}^{[N]}$ has the distribution:

$$p(\hat{v}^{[N]} = k^{-1}) = 1 - b^N$$

$$p(\hat{v}^{[N]} = 0) = b^N \tag{S.8}$$

16

In this way, for each temporal repetition, the locomotor would either achieve nominal velocity (with probability $1 - b^N$) or stay in place (b^N). Now we consider the matter transportation task including multiple temporal repetitions (temporal redundancy). Consider each temporal repetition as an independent trial, so that $\hat{D}$ follows a binomial distribution.

From definition, we only declare matter transportation to be successful if every step achieves nominal velocity. The probability of an overall successful matter transportation task ($\hat{D} = D$) is connected to the probability of a successful individual task by:

$$p(\hat{v} = k^{-1}) = \sqrt[T]{p_0}, \tag{S.9}$$

where $p(\hat{v} = k^{-1})$ is the probability of successful matter transportation in each trial; and $T = kD$ is the number of trials (temporal repetition).

Combining equation (S.9) with the first equation in (S.8), we have

$$b^N = 1 - (p_0)^{1/(kD)}.$$

It follows that

$$N = \frac{\log(1 - p_0^{1/(kD)})}{\log(b)} \tag{S.10}$$

We refer the reader to Figure 3E in the text for a plot of N as a function of b. We acknowledge that our choice of $f(t)$ might not facilitate the tightest bound on N. Yet we illustrate that N is at least bounded by a logarithm function (Eq. S.10):

$$N_{p_0} \leq \frac{\log(1 - p_0^{1/(kD)})}{\log(b)} \tag{S.11}$$

$\square$

Proposition 6. *Consider a matter transportation task to deliver a payload over distance D at the scheduled time of arrival $T = kD$, where k^{-1} is the nominal speed. Define the*

matter transportation task to be successful if the actual displacement $\hat{D}$ (evaluated at T) satisfies $|D - \hat{D}| < \epsilon$. Now we consider a non-zero $\epsilon > 0$. To guarantee successful matter transportation with probability p_0, "the minimal spatial redundancy" is bounded by:

$$N_{\epsilon, p_0} \leq N_{p_0}$$

Proof. Following the proof in Proposition 5, for the total of $T = kD$ repetitions, we define m to be the tolerable number of failed trials; m is related to ϵ by: $m = \lfloor k\epsilon \rfloor$, where $\lfloor \rfloor$ is the floor operator. In this way, we have:

$$p_0 = \sum_{j=0}^{m} \binom{kD}{j} \left(1 - p(\hat{v} = k^{-1}) \right)^{j} \left(p(\hat{v} = k^{-1}) \right)^{kD-j}$$

where $p(\hat{v} = k^{-1})$ is the probability of successful matter transportation in each trial; and $T = kD$ is the number of trials (temporal repetition). We then design B as a function mapping from the probability of overall successful matter transportation to a successful individual task:

$$p(\hat{v} = k^{-1}) = B(p_0, m, kD).$$

From algebra, we know that

$$B(p_0, m, kD) \leq B(p_0, 0, kD) = p_0^{1/(kD)},$$

from which we know that $N_{\epsilon, p_0} \leq N_{p_0}$

$\square$

3 Movie S1 caption

Content	Time
Outdoor experiments	
Large rocks	0:10
Pine straws	0:35
Grass	0:53
Gravel pavement	1:17
Laboratory experiments	
Laboratory experiments	1:41
Experimental verification	
Contact errors from terrain rugosity	2:03
Estimated time of arrival	2:17
Self-transport punctuality	3:44
Locomotion failure	4:16
Contact modulation	4:56

Section 1: Robot outdoor experiments

0:10-0:34: A 12-legged robot successfully self-transporting over large rocks. (Inset) A 6-legged robot experiencing thrust deficiency (and thus degraded locomotion performance) in this environment.

0:35-0:53: A 12-legged robot successfully self-transporting through entangled granular material (pine straw).

0:53-1:15: A 12-legged robot successfully self-transporting over a grass field (uphill and downhill).

1:17-1:41: A 12-legged robot successfully self-transporting over gravel pavement.

Section 2: Robot laboratory experiments

1:41-2:03: A 12-legged robot successfully self-transporting over challenging laboratory terrain including tall obstructions, large bricks, 15° slope, different surface frictions, an array of posts, natural debris, and granular material.

Section 3: Experimental verification of the framework

2:03-2:17: Side-view videos of a 12-legged robot on a rugose terrain. A few legs experience bac contamination which results in degradation in speed.

2:17-3:44: Top-view videos of (*top*) an 8-legged robot, (*mid*) a 12-legged robot, and (*bottom*) a 16-legged robot self-transport over rugose terrain with $R_g = \{0,\ 0.17,\ 0.32\}$. These robots have similar locomotion speed on the flat terrain ($R_g = 0$). The advantage of having greater spatial redundancy emerges when locomoting on terrains with greater rugosity.

3:44-4:16: Top-view videos of (*top*) a 6-legged robot and (*mid*) a 14-legged robot self-transporting over rugose terrains.

4:17-4:55: Side-view of a 6-legged robot becoming "stuck" due to sufficiently large terrain rugosity. The robot eventually escapes due to sufficient temporal redundancy.

4:56-5:31: Side-view of a 12-legged robot with contact modulation (CM) self-transporting over rugose terrain with $R_g = \{0,\ 0.17,\ 0.32\}$.

References and Notes

1. J. Aguilar, D. Monaenkova, V. Linevich, W. Savoie, B. Dutta, H.-S. Kuan, M. D. Betterton, M. A. D. Goodisman, D. I. Goldman, Collective clog control: Optimizing traffic flow in confined biological and robophysical excavation. *Science* **361**, 672–677 (2018). doi:10.1126/science.aan3891 Medline

2. J. Mindell, H. Rutter, S. Watkins, *Encyclopaedia of Environmental Health* (Elsevier Masson, 2011), pp. 578–589.

3. H. Kreutzmann, The Karakoram Highway: The Impact of Road Construction on Mountain Societies. *Mod. Asian Stud.* **25**, 711–736 (1991). doi:10.1017/S0026749X00010817

4. R. M. Alexander, Principles of animal locomotion (Princeton Univ. Press, 2003).

5. P. Holmes, R. J. Full, D. Koditschek, J. Guckenheimer, The Dynamics of Legged Locomotion: Models, Analyses, and Challenges. *SIAM Rev.* **48**, 207–304 (2006). doi:10.1137/S0036144504445133

6. M. Raibert, K. Blankespoor, G. Nelson, R. Playter, *IFAC Proceedings Volumes* **41**, 10822 (2008).

7. U. Saranli, M. Buehler, D. E. Koditschek, RHex: A Simple and Highly Mobile Hexapod Robot. *Int. J. Robot. Res.* **20**, 616–631 (2001). doi:10.1177/02783640122067570

8. M. G. Bekker, *Off-the-road locomotion: Research and development in terramechanics* (Univ. of Michigan Press, 1960).

9. C. Li, T. Zhang, D. I. Goldman, A terradynamics of legged locomotion on granular media. *Science* **339**, 1408–1412 (2013). doi:10.1126/science.1229163 Medline.

10. C. Li, A. O. Pullin, D. W. Haldane, H. K. Lam, R. S. Fearing, R. J. Full, Terradynamically streamlined shapes in animals and robots enhance traversability through densely cluttered terrain. *Bioinspir. Biomim.* **10**, 046003 (2015). doi:10.1088/1748-3190/10/4/046003 Medline

11. W. Weber, E. Weber, *Mechanik der menschlichen Gehwerkzeuge* (Verlag der Dietrichschen Buchhandlung, Göttingen, Germany, 1836).

12. J. Lee, J. Hwangbo, L. Wellhausen, V. Koltun, M. Hutter, Learning quadrupedal locomotion over challenging terrain. *Sci. Robot.* **5**, eabc5986 (2020). doi:10.1126/scirobotics.abc5986 Medline

13. J. Borenstein, H. R. Everett, L. Feng, D. Wehe, Mobile robot positioning: Sensors and techniques. *J. Robot. Syst.* **14**, 231–249 (1997). doi:10.1002/(SICI)1097-4563(199704)14:4<231:AID-ROB2>3.0.CO;2-R

14. M. Hutter *et al.*, *2016 IEEE/RSJ international conference on intelligent robots and systems (IROS)* (IEEE, 2016), pp. 38–44.

15. E. R. Westervelt, J. W. Grizzle, C. Chevallereau, J. H. Choi, B. Morris, *Feedback control of dynamic bipedal robot locomotion* (CRC press, 2018).

16. Y. Ozkan-Aydin, D. I. Goldman, Self-reconfigurable multilegged robot swarms collectively accomplish challenging terradynamic tasks, *Science Robotics* **6**, eabf1628 (2021).

17. S. Aoi, T. Tanaka, S. Fujiki, T. Funato, K. Senda, K. Tsuchiya, Advantage of straight walk instability in turning maneuver of multilegged locomotion: A robotics approach. *Sci. Rep.* **6**, 30199 (2016). doi:10.1038/srep30199 Medline

18. E. Moore, D. Campbell, F. Grimminger, M. Buehler, *Proceedings 2002 IEEE International Conference on Robotics and Automation (Cat. No. 02CH37292)*, Washington, DC, 11 to 15 May, 2002 (IEEE, 2002), vol. 3, pp. 2222–2227.

19. C. Ordonez, J. Shill, A. Johnson, J. Clark, E. Collins, Unmanned Systems Technology XV. *Proc SPIE Int Soc Opt Eng* **8741**, 240–251 (2013).

20. X. A. Wu, T. M. Huh, R. Mukherjee, M. Cutkosky, Integrated Ground Reaction Force Sensing and Terrain Classification for Small Legged Robots. *IEEE Robot. Autom. Lett.* **1**, 1125–1132 (2016). [doi:10.1109/LRA.2016.2524073](doi:10.1109/LRA.2016.2524073)

21. C. E. Shannon, A Mathematical Theory of Communication. *Bell Syst. Tech. J.* **27**, 379–423 (1948). [doi:10.1002/j.1538-7305.1948.tb01338.x](doi:10.1002/j.1538-7305.1948.tb01338.x)

22. A. Feinstein, A new basic theorem of information theory. *IEEE Trans. Inf. Theory* **4**, 2– 22 (1954).

23. R. J. Full, D. E. Koditschek, Templates and anchors: Neuromechanical hypotheses of legged locomotion on land. *J. Exp. Biol.* **202**, 3325–3332 (1999). [doi:10.1242/jeb.202.23.3325](doi:10.1242/jeb.202.23.3325) Medline

24. H. C. Astley, C. Gong, J. Dai, M. Travers, M. M. Serrano, P. A. Vela, H. Choset, J. R. Mendelson 3rd, D. L. Hu, D. I. Goldman, Modulation of orthogonal body waves enables high maneuverability in sidewinding locomotion. *Proc. Natl. Acad. Sci. U.S.A.* **112**, 6200–6205 (2015). doi:10.1073/pnas.1418965112 Medline

25. H. Forssberg, Stumbling corrective reaction: A phase-dependent compensatory reaction during locomotion. *J. Neurophysiol.* **42**, 936–953 (1979). [doi:10.1152/jn.1979.42.4.936](doi:10.1152/jn.1979.42.4.936) Medline

26. P. E. Schiebel *et al*., Robophysical modeling of bilaterally activated and soft limbless locomotors, *Biomimetic and Biohybrid Systems: 9th International Conference, Living Machines*, Freiburg, Germany, 28 to 30 July, 2020 (Springer International Publishing, 2020), pp. 300–311.

27. B. Chong, J. He, S. Li, E. Erickson, K. Diaz, T. Wang, D. Soto, D. I. Goldman, Self-propulsion via slipping: Frictional swimming in multilegged locomotors. *Proc. Natl. Acad. Sci. U.S.A.* **120**, e2213698120 (2023). doi:10.1073/pnas.2213698120 Medline

28. D. Zhao, B. Bittner, G. Clifton, N. Gravish, S. Revzen, Walking is like slithering: A unifying, data-driven view of locomotion. *Proc. Natl. Acad. Sci. U.S.A.* **119**, e2113222119 (2022). doi:10.1073/pnas.2113222119 Medline

29. J. R. Pierce, *An Introduction to Information Theory: Symbols, Signals and Noise* (Courier Corporation, 2012).

30. B. Chong, Y. O Aydin, J. M. Rieser, G. Sartoretti, T. Wang, J. Whitman, A. Kaba, E. Aydin, C. McFarland, K. Diaz Cruz, J. W. Rankin, K. B. Michel, A. Nicieza, J. R. Hutchinson, H. Choset, D. I. Goldman, A general locomotion control framework for multi-legged

locomotors. *Bioinspir. Biomim.* **17**, 046015 (2022). [doi:10.1088/1748-3190/ac6e1b](doi:10.1088/1748-3190/ac6e1b) Medline

31. Y. Ozkan-Aydin, B. Chong, E. Aydin, D. I. Goldman, *2020 3rd IEEE International Conference on Soft Robotics (RoboSoft)*, New Haven, CT, USA, 15 May to 15 July, 2020 (IEEE, 2020), pp. 156–163.

32. A. Jacoff, A. Downs, A. Virts, E. Messina, *Proceedings of the 8th Workshop on Performance Metrics for Intelligent Systems*, Gaithersburg, MD, USA, 19 to 21 August, 2008 (NIST, 2008), pp. 29–34.

33. B. Chong, T. Wang, J. M. Rieser, B. Lin, A. Kaba, G. Blekherman, H. Choset, D. I. Goldman, Frequency modulation of body waves to improve performance of sidewinding robots. *Int. J. Robot. Res.* **40**, 1547–1562 (2021). [doi:10.1177/02783649211037715](doi:10.1177/02783649211037715)

34. J. Whitman, N. Zevallos, M. Travers, H. Choset, *2018 IEEE International Symposium on Safety, Security, and Rescue rRobotics (SSRR)*, Philadelphia, PA, USA, 6 to 8 August, 2018 (IEEE, 2018), pp. 1–6.

35. N. D. Naclerio, A. Karsai, M. Murray-Cooper, Y. Ozkan-Aydin, E. Aydin, D. I. Goldman, E. W. Hawkes, Controlling subterranean forces enables a fast, steerable, burrowing soft robot. *Sci. Robot.* **6**, eabe2922 (2021). doi:10.1126/scirobotics.abe2922 Medline

36. J. J. Abbott, Z. Nagy, F. Beyeler, B. J. Nelson, Robotics in the Small, Part I: Microbotics. *IEEE Robot. Autom. Mag.* **14**, 92–103 (2007). [doi:10.1109/MRA.2007.380641](doi:10.1109/MRA.2007.380641)

37. S. Tatikonda, S. Mitter, The Capacity of Channels With Feedback. *IEEE Trans. Inf. Theory* **55**, 323–349 (2008). [doi:10.1109/TIT.2008.2008147](doi:10.1109/TIT.2008.2008147)

38. C. Lott, O. Milenkovic, E. Soljanin, *2007 IEEE Information Theory Workshop on Information Theory for Wireless Networks*, Bergen, Norway, 1 to 7 July, 2007 (IEEE, 2007), pp. 1–5.

39. B. Chong, T. Wang, E. Erickson, P. J. Bergmann, D. I. Goldman, Coordinating tiny limbs and long bodies: Geometric mechanics of lizard terrestrial swimming. *Proc. Natl. Acad. Sci. U.S.A.* **119**, e2118456119 (2022). doi:10.1073/pnas.2118456119 Medline

40. D. S. Marigold, Role of peripheral visual cues in online visual guidance of locomotion. *Exerc. Sport Sci. Rev.* **36**, 145–151 (2008). [doi:10.1097/JES.0b013e31817bff72](doi:10.1097/JES.0b013e31817bff72) Medline

41. T. Krasovsky, A. Lamontagne, A. G. Feldman, M. F. Levin, Effects of walking speed on gait stability and interlimb coordination in younger and older adults. *Gait Posture* **39**, 378–385 (2014). doi:10.1016/j.gaitpost.2013.08.011 Medline

42. K. Diaz, E. Erickson, B. Chong, D. Soto, D. I. Goldman, Active and passive mechanics for rugose terrain traversal in centipedes. *J. Exp. Biol.* **226**, jeb244688 (2023). [doi:10.1242/jeb.244688](doi:10.1242/jeb.244688) Medline

43. S. Sponberg, R. J. Full, Neuromechanical response of musculo-skeletal structures in cockroaches during rapid running on rough terrain. *J. Exp. Biol.* **211**, 433–446 (2008). [doi:10.1242/jeb.012385](doi:10.1242/jeb.012385) Medline

44. B. Bläsing, H. Cruse, Mechanisms of stick insect locomotion in a gap-crossing paradigm. *J. Comp. Physiol. A Neuroethol. Sens. Neural Behav. Physiol.* **190**, 173–183 (2004). doi:10.1007/s00359-003-0482-3 Medline

45. D. Soto, B. Chong, Code for rugose terrain generation, Zenodo (2021); https://doi.org/10.5281/zenodo.7121219

46. D. L. Hu, J. Nirody, T. Scott, M. J. Shelley, The mechanics of slithering locomotion. *Proc. Natl. Acad. Sci. U.S.A.* **106**, 10081–10085 (2009). doi:10.1073/pnas.0812533106 Medline

47. A. Gut, *Probability: a graduate course* (Springer, ed. 2, 2005).